A universal mode of helix packing in RNA

Elizabeth A. Doherty[1], Robert T. Batey[1,2], Benoît Masquida[1,2] and Jennifer A. Doudna[1,2]

[1]Department of Molecular Biophysics and Biochemistry and [2]Howard Hughes Medical Institute, Yale University, New Haven, Connecticut 06520, USA.

RNA molecules fold into specific three-dimensional shapes to perform structural and catalytic functions. Large RNAs can form compact globular structures, but the chemical basis for close helical packing within these molecules has been unclear. Analysis of transfer, catalysis, *in vitro*-selected and ribosomal RNAs reveal that helical packing predominantly involves the interaction of single-stranded adenosines with a helix minor groove. Using the *Tetrahymena thermophila* group I ribozyme, we show here that the near-perfect shape complementarity between the adenine base and the minor groove allows for optimal van der Waals contacts, extensive hydrogen bonding and hydrophobic surface burial, creating a highly energetically favorable interaction. Adenosine is recognized in a chemically similar fashion by a combination of protein and RNA components in the ribonucleoprotein core of the signal recognition particle. These results provide a thermodynamic explanation for the noted abundance of conserved adenosines within the unpaired regions of RNA secondary structures.

RNA helical packing commonly involves two general types of base triples (termed Type I and Type II) between the minor groove surfaces of unpaired adenosines and base pairs[1] (Table 1). Two sets of these tandem Type I/II base triples stabilize the P4-P6 domain of the *Tetrahymena* group I intron[2] (Fig. 1). In Type I (occurring at A153, A184 and A186 of P4-P6), the N1, C2, N3 and 2′ hydroxyl group along the minor groove face of the adenosine contact the entire minor groove surface of a base pair, including both ribose sugars (Fig. 1*a*,*b*). Type I allows the burial of ~195 Å^2, ~30% more molecular surface area than other base triples, suggesting that it is a particularly favorable tertiary interaction. Residues A152 and A183 stack above A153 and A184, respectively, and each form Type II interactions (Fig. 1*a*). In Type II, the N1, C2, N3 and 2′ hydroxyl group of the adenosine contact approximately one-half of the minor groove of a base pair, allowing the burial of ~145 Å^2 of molecular surface (Fig. 1*c*). Single Type I interactions and consecutive Type I/II interactions, in which the 5′ adenosine forms Type II and the 3′ adenosine forms Type I interactions, occur in nearly all of the known structures of RNAs and RNA–protein complexes[2–14] (Table 1). In contrast, Type II base triples are rarely observed outside the Type I/II motif. Furthermore, tertiary interactions involving the ubiquitous GAAA tetraloop depend on consecutive Type I/II interactions mediated by the final two adenosines of the tetraloop[12,15] (Table 1; A152 and A153 in P4–P6).

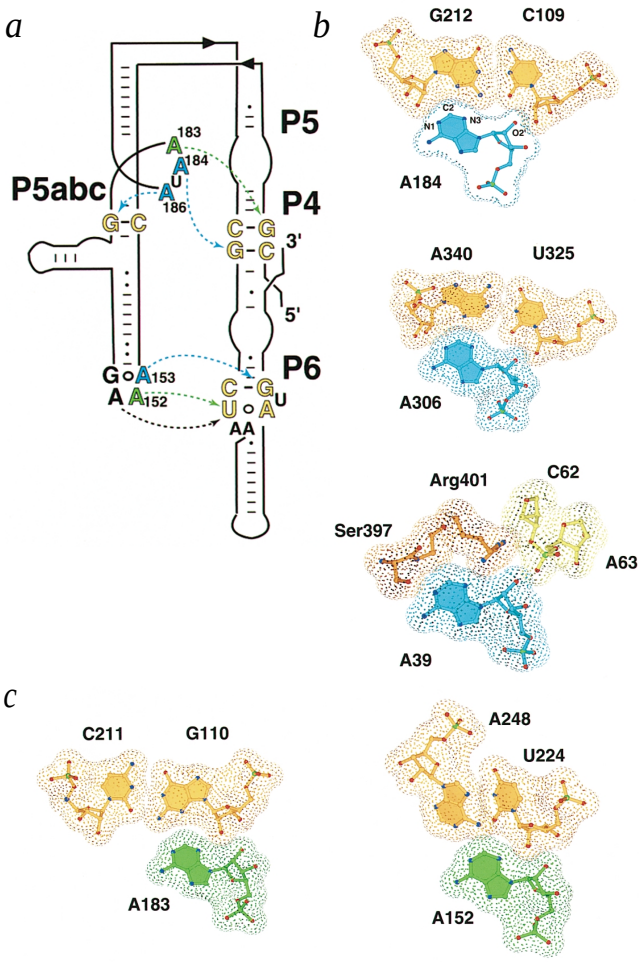

Fig. 1 Type I and Type II base triples. ***a***, Adenosines that form Type I and Type II base triple interactions in the P4–P6 domain of the Tetrahymena group I intron[2] are labeled in cyan and green, respectively. ***b***, Examples of base triple Type I from P4–P6 (A184•C109–G212) and *H. marismortui* 23S rRNA (A306•U325–340) (ref. 11) and a Type I-like interaction involving protein and RNA components from the signal recognition particle (A39•Ser 397–Arg 401–C62–A63) (ref. 22). The adenosine N1, C2, N3 and 2′ hydroxyl (O2′) groups interact with the entire minor groove surface of the base pairs, including both riboses. The strands containing A184 and A306 are locally antiparallel to the strands containing C109 and U325. ***c***, Examples of Type II base triples between adenosines and Watson-Crick C–G and Hoogsteen A–U base pairs in the P4–P6 domain. The adenosine N1, C2, N3 and 2′ hydroxyl groups interact with one-half of the minor groove surface of the base pair. The adenosine is oriented locally antiparallel to the strand (containing G110 or U224) with which it primarily interacts.

Thermodynamic analysis

To understand the energetic basis for the prevalence of these base triples, we performed a mutational analysis of the Type I/II interaction involving A183 and A184 of the P4–P6 domain. We examined the effects of mutations on domain stability using a system in which P4–P6 assembles from two separate molecules: the independently folded P5abc subdomain and a mutant ribozyme called $E^{\Delta P5abc}$ (ref. 16) (Fig. 2*a*). This two piece system allows for the binding of P5abc to the $E^{\Delta P5abc}$ ribozyme to be measured using a native gel electrophoresis mobility shift assay. Footprinting experiments using the chemical probe Fe(II)-EDTA showed that mutations of residues forming these base triples did not affect the structure of P5abc or $E^{\Delta P5abc}$, with the exception of the C109–G212 base pair in helix P4 (data not shown). Thus, the energetic effects of these mutations should result primarily from disruption of the Type I and Type II base triples rather than misfolding of P5abc or $E^{\Delta P5abc}$. The GAAA tetraloop-mediated Type I/II interaction (involving A152 and A153) was not examined, as mutations within this motif are expected to disrupt the structure of the tetraloop or its receptor helix[15] (Fig. 1*a*).

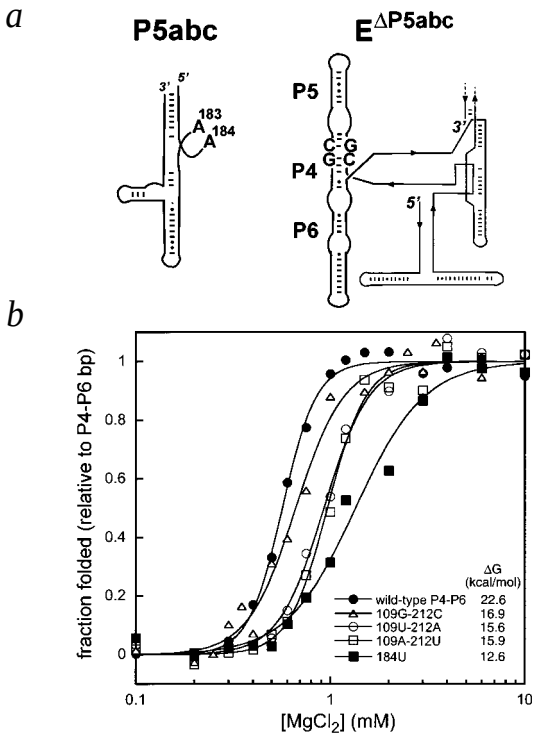

Fig. 2 Energetics of Type I and Type II interactions. ***a***, The P5abc and $E^{\Delta P5abc}$ RNAs used in gel mobility shift assays to generate the data shown in Table 2. Both isolated RNAs fold into native-like structures at 10 mM $MgCl_2$, and, therefore, the measured binding affinities strictly reflect the interaction of P5abc with $E^{\Delta P5abc}$ (ref. 16). ***b***, Folding of mutants of the P4–P6 domain RNA as a function of $MgCl_2$ concentration relative to an unfolded control RNA, P4–P6 bp, monitored by polyacrylamide gel electrophoresis[18]. From this analysis, the $[Mg^{2+}]_{1/2}$ values and Hill coefficients (see Methods), respectively, were determined to be 0.56 and 5.1 for wild type P4–P6 (109C–212G), 0.66 and 3.9 for P4–P6 109G–212C, 0.96 and 3.8 for P4–P6 109U–212A, 0.99 and 3.9 for P4–P6 109A–212U, and 1.3 and 3.2 for P4–P6 184U. The $[Mg^{2+}]_{1/2}$ value and Hill coefficient for wild type P4–P6 are the average values calculated from four separate titration curves. A single titration curve was generated for all other RNAs. Free energy of dissociation (ΔG) values were derived from midpoints of these titration curves (see Methods).

Previous mutational analysis showed that hydrogen bonds mediated by 2′ hydroxyl groups within Type I and Type II base triples make modest energetic contributions towards the stabilization of the interactions (0.2–1.0 kcal mol^{-1} in P4–P6)[17,18]. Using a native gel mobility shift assay to measure the affinities of wild type and mutant P5abc subdomain RNAs for $E^{\Delta P5abc}$ RNA (see Methods), we obtained similar results for 2′ deoxy substitutions of residues A183 and A184 in P5abc (Table 2). In stark contrast, mutation of either of these residues to U or C results in a loss of between one-third and one-half of the total apparent binding free energy of the P5abc–$E^{\Delta P5abc}$ complex ($\Delta\Delta G$ = 4.3–6.6 kcal mol^{-1}; Table 2). Models of the pyrimidine mutants suggest that these effects result from a reduction in van der Waals surface–surface contacts and from creation of unfavorable electrostatic interactions due to the effective replacement of the adenine C2 hydrogen by a carbonyl group. Although a pyrimidine can be accommodated in a Type I-like interaction, this triple is much less thermodynamically stable, perhaps due to the requirement for bridging waters to form the complete set of hydrogen bonds seen with adenosine[19].

To examine the effect of altering the van der Waals interaction between the adenosine and the minor groove, A183 and A184 were mutated to G and 2-amino purine (2AP). Molecular modeling predicts that the bulky exocyclic amino group at the

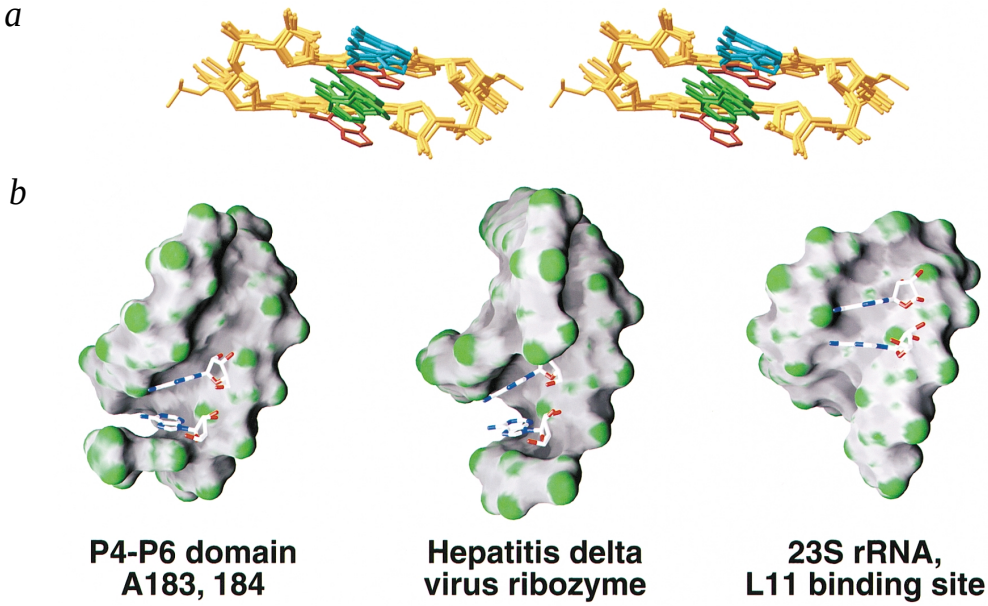

Fig. 3 Comparison of Type I/II base triples from different RNAs. ***a***, Superposition of consecutive Type I/II base triples from the 23S rRNA from *H. marismortui* [PDB entry code 1FFK][11]. The ribose-phosphate backbone of the helices (gold) from 10 individual examples of this interaction with nonidentical sequences were superimposed using LSQMAN[33], with a r.m.s. deviation of 1.40 Å. Six individual structures from this family are shown in stereo, with the coloring scheme of the helix and adenosines consistent with Fig. 1. The adenosines from one structure have been colored red to emphasize that the two adenosines remain stacked, irrespective of their orientation relative to the helix minor groove. ***b***, Surface representations of adenosines within Type I/II base triples docked into the minor groove from (left to right) the P4–P6 domain (the A183 and A184 mediated interaction)[2], the hepatitis delta virus ribozyme[4] and the L11 protein–RNA complex[6]. Nucleotides that stack upon the adenosines are included within the molecular surface of the P4–P6 and hepatitis delta virus figures. This figure was created with GRASP[34].

C2 position of these bases should sterically occlude docking of the base into the minor groove. In fact, G and 2AP mutations caused a significant disruption of each of the base triple interactions ($\Delta\Delta G$ = 3.2–4.0 kcal mol^{-1}; Table 2). In contrast, substitution of A183 and A184 with inosine (I) and purine (P), which lack the exocyclic amino group, supported tight binding of the P5abc–$E^{\Delta P5abc}$ complex ($\Delta\Delta G$ = 0.8–1.7 kcal mol^{-1}; Table 2). The modest energetic penalties of these substitutions may reflect differences in stacking energies of purine bases with different substituents at the C6 position, as measured for purine nucleosides and bases in water[20], indicating that base stacking contributes to this interaction. These results suggest that surface complementarity between the adenine base and the minor groove, which optimizes a combination of van der Waals, electrostatic and hydrogen bonding contacts, is a major determinant of this high affinity interaction.

Table 1 Examples of consecutive type I/II base triples[1]

RNA	Structural context	Type	Interacting bases
P4–P6 domain	Internal bulge/helix	II	A183 • G110–C211
		I	A184 • C109–G212
P4-P6 domain	GAAA tetraloop/ tetraloop receptor	II	A152 • U224 ∘ A248
		I	A153 • C223–G250
Hepatitis delta virus ribozyme	Internal bulge/helix	II	A77 • C119–G128
		I	A78 • C118–G129
L11 protein/ RNA complex	Internal bulge/helix	II	A1084 • C/U1105–G/A1054
		I	A1085 • C1104–G1055
Hammerhead ribozyme	GAAA tetraloop/ helix	II	A23 • C10.4–G11.4
		I	A24 • C10.3–G11.3

[1]Watson-Crick base pairs are denoted with a dash between the bases while Hoogsteen base pairs are denoted with an open dot between the bases. Closed dots separate the base pairs from the unpaired adenosines with which they interact. Arrows indicate direction of strands. All observed Type I/II interactions contain the same relative strand directions as the examples shown here.

Sequence specificity of adenosine interactions

To determine if the Type I and Type II adenosines contact helices in a sequence specific manner, we mutated each of the base pairs involved in the A183 and A184 mediated interactions to all other Watson-Crick pairs. $E^{\Delta P5abc}$ RNAs in which the G110–C211 pair was mutated to C–G, U–A and A–U bound to P5abc with near wild type affinity, suggesting that the Type II adenosine docks against the minor groove with little sequence specificity (Table 2). This is likely due to the fact that in Type II, the adenosine is positioned to contact only one-half of the minor groove surface (Fig. 1*c*). We further examined binding of all three mutant $E^{\Delta P5abc}$ RNAs to P5abc RNAs containing A183G, A183C and A183U point mutations to determine if any other combinations of bases support Type II-like interactions. The A183U and A183C P5abc RNAs bound poorly to the wild type and all three $E^{\Delta P5abc}$ mutant constructs (not shown). However, A183G P5abc bound to $E^{\Delta P5abc}$ RNAs containing C–G or U–A substitutions for the G110–C211 base pair with affinities similar to the wild type P5abc–$E^{\Delta P5abc}$ interaction (Table 2). Supporting this result, phylogenetic covariation analysis of 23 Type II base triples in 23S rRNA shows that C–G and U–A base pairs correlate with a tolerance for both A and G at the location of the Type II adenosine (see Methods).

The C109–G212 base pair of the Type I interaction could not be mutated within $E^{\Delta P5abc}$ without disrupting other tertiary interactions required for $E^{\Delta P5abc}$ folding[21] (data not shown). Therefore, we assessed the effects of mutating this base pair using a more qualitative assay involving folding of the isolated P4–P6 domain as a function of magnesium ion concentration[18]. Our results show that the adenosine in Type I has an energetic preference for the C109–G212 base pair over all other base pairs in this position (Fig. 2*b*), for reasons that are not clear. Interestingly, this preference is supported by phylogenetic covariation analysis of Type I triples (see below).

Protein recognition of adenosine in RNA

The minor groove face of an adenosine residue is recognized by a protein–RNA interface within the core of the signal recognition particle (SRP)[22] in a nearly identical fashion to the adenosine in the Type I base triple (Fig. 1*b*). The universally conserved residue A39 in an asymmetric internal loop of the 4.5S RNA interacts with Ser and Arg side chains of the SRP protein, Ffh, and the ribose-phosphate backbone from another region of the RNA. Residue A39 of the SRP is placed in a pocket that has a shape and electrostatic potential strikingly similar to that of the minor groove of a Watson-Crick base pair (Fig. 1*b*).

To compare protein-based recognition of A39 with RNA-based recognition of A184, we constructed a series of adenosine mutations within the 4.5S RNA similar to those constructed in the P4-P6 domain and used a filter binding assay (see Methods) to measure the energetics of dissociation of these mutant RNAs with the RNA binding domain of the Ffh protein. The general trend of these mutations is similar to that of mutations in A184 of the P4–P6 domain (Table 2). Mutation of A39 to G or 2AP resulted in a loss in the apparent binding free energy of the protein–RNA complex that is almost identical to that of a mutant (ΔASL) in which the entire asymmetric internal loop of the 4.5S RNA is deleted. This implies that addition of an exocyclic amino group along the minor groove interface destroys the interaction. These results suggest that the key to specific adenosine recognition, whether by protein or RNA, is the creation of a complementary binding surface.

Phylogenetic analysis

Within the 2,900-nucleotide *Haloarcula marismortui* 23S rRNA[11], 26 Type I/II interactions as well as several single Type I base triples are found[23]. In the 16S rRNA from *Thermus thermophilus*, 10 examples of Type I/II interactions and at least three examples of isolated Type I triples occur[13]. Strikingly, Type I/II base triples account for about one-third of all consecutive adenosines in the 23S RNA that are at least 90% conserved and the majority of those involved in RNA tertiary interactions (ref. 11; *http://www.rna.icmb.utexas.edu*), underscoring the critical importance of this mode of helical packing to RNA stability.

Table 2 Mean apparent ΔΔG of P5abc–E$^{\Delta P5abc}$ and 4.5S RNA–Ffh complexes[1]

P5abc or E$^{\Delta P5abc}$ mutant	ΔΔG (kcal mol^{-1})
184 deoxy	1.4
A184C	6.6
A184U	5.8
A184G	3.4
A184I	0.8
A184–2AP	4.0
A184P	1.2
A183 deoxy	0.6
A183C	5.2
A183U	4.3
A183G	3.2
A183I	1.3
A183–2AP	3.9
A183P	1.7
110C–211G	0.2
110U–211A	0.3
110A–211U	1.0
110C–211G A183G	1.1
110U–211A A183G	0.6
110A–211U A183G	2.2
4.5S RNA mutant	**ΔΔG (kcal mol^{-1})**
A39 deoxy	1.8
A39C	3.6
A39G	4.8
A39I	0.8
A39–2AP	4.2
A39P	0.7
ΔASL	5.2

[1]The ΔG of the P5abc–E$^{\Delta P5abc}$ wild type complex was 14.1 kcal mol^{-1} while that of the 4.5S RNA–Ffh M domain complex was 14.2 kcal mol^{-1}. All ΔG values were derived from fits of binding data to a Langmuir isotherm (see Methods), using the equation $\Delta G = -RT\ln(K_d)$. $\Delta\Delta G = \Delta G_{wildtype} - \Delta G_{mutant}$. Error for ΔΔG values is ± 0.6 kcal mol^{-1}.

Results of phylogenetic covariation analysis of 23 Type I/II interactions from 23S rRNA (see Methods) are in accord with the thermodynamic data presented above. When the adenosine of Type I interacts with a Watson-Crick base pair, C–G (such that strands containing A and C are locally antiparallel; Table 1, Fig. 1*b*) is strongly preferred (89% of all examples), followed by G–C (6%), and A–U and U–A (2.5% each). Type II base triples involving Watson-Crick pairs are less sequence specific, with C–G (such that strands containing A and C are locally antiparallel; Table 1, Fig. 1*c*) preferred (69%) followed by U–A (13%), and G–C and A–U (9% each). An examination of Watson-Crick base pair frequencies within 21 of these Type I/II base triples using a significantly larger data set of aligned sequences (see Methods) revealed a similar pattern (Type I: CG = 76%, GC = 13%, UA = 8%, AU = 3%; Type II: CG = 63%, GC = 8%, UA = 18%, AU = 11%). In these analyses the Type II base triple shows more sequence specificity than expected based on the thermodynamic analysis. However, our results do not account for the effect of the helix sequence on its stability and geometry or for constraints on sequence imposed by functional requirements. Despite these observed sequence preferences, it has not been possible to predict the locations of the interacting partners of Type I or consecutive Type I/II base triples except in contexts in which additional stringent sequence requirements are imposed[15,24].

Energetic stability of Type I/II and Type I interactions

The small energetic preference for the receptor base pair in Type I and II triples could have functional consequences. For example, A1492 and A1493 in the decoding site of the 30S ribosomal subunit may use Type I/II triples to scan for correct Watson-Crick helix formation between codons and anticodons[25,26]. This would be consistent with the idea that the A-form geometry of the host helix, rather than base pair identity, is the principle recognition determinant of the Type I/II interaction.

Type I/II interactions provide significant energetic stability to RNA folds, as reflected by the extensive burial of the molecular surface from solvent allowed by the interaction. Formation of Type I base triples buries an average of 195 Å^2 ± 15 of surface area (from 33 examples within a variety of RNAs)[2–14], compared to an average of 150 Å^2 ± 30 for all other base triples within several RNA structures[2–6]. While analysis of individual Type I and Type II base triples indicates that the motif optimizes surface area burial, stacking of the adenosines hydrogen bonding between each adenosine and the minor groove is frequently not optimized, allowing the adenosine to approach the minor groove from a variety of angles (Fig. 3*a*). Thus, this mode of helical packing adjusts to local conformations, allowing the adenosines to interact with a variety of minor groove surfaces (Fig. 3*b*).

The shallow and accessible minor groove is the optimal surface upon which to build higher order structure in RNA. The Type I/II interaction dominates the folding of a wide variety of RNAs, consistent with the thermodynamic analysis of the interaction presented here. This explains the long-standing observation that adenosines account for the majority of residues within the single-stranded segments that mediate higher order RNA folding[24,27,28].

Methods

Gel mobility shift experiments. Gel mobility shift experiments were performed and quantified as described[16]. Briefly, a trace quantity (< 10 pM) of radiolabeled P5abc RNA was incubated with unlabeled E$^{\Delta P5abc}$ RNA in 1× Tris-MES-EDTA (TME) buffer (33 mM Tris, 66 mM MES, 0.1 mM Na_2EDTA, pH 6.0), 4% (v/v) glycerol, 30 mM KCl and 10 mM $MgCl_2$ at 37 °C for 24 h to establish equilibrium. Gels were run in 1× TME, 30 mM KCl and 10 mM $MgCl_2$ at 37 °C. After drying, gels were visualized with a Fuji phosphorimager and bands corresponding to free and bound P5abc were quantified with associated software. The fraction of P5abc bound by E$^{\Delta P5abc}$ was determined by dividing the intensity of the unshifted (free) P5abc by the total intensity of P5abc in the gel lane. Typically, > 95% of radiolabeled P5abc was bound to E$^{\Delta P5abc}$ at saturation. Least squares fits were to a single-site binding equation: $f = (a - b) \times ([E^{\Delta P5abc}] / ([E^{\Delta P5abc}] + K_d)) + b$, where a is the maximum fraction of P5abc bound at saturation, b is the amount of P5abc apparently bound in the absence of E$^{\Delta P5abc}$ (accounting for background) and K_d is the apparent equilibrium dissociation constant. The concentration of radiolabeled P5abc was at least 10-fold below the K_d in all experiments.

P4–P6 polyacrylamide gel folding assays. These assays were conducted as described[18]. Polyacrylamide gel electrophoresis was used to monitor folding of P4–P6 into a compact shape as the P5abc region docks into the P5–P4–P6 helical stack (see Figs 1*a*, 2*a*). The mobilities of each P4–P6 construct were measured relative to those of a P4–P6 mutant called P4–P6 bp, which was unfolded due to the presence of Watson-Crick base pairs in the sequence linking the P5abc and P5–P4–P6 segments. Thus, in P4–P6 bp, no interaction occurs between P5abc and P5–P4–P6. All experiments were fit to the Hill equation. The $[Mg^{2+}]_{1/2}$ values and Hill coefficients were calculated from fits of the data to the Hill equation: $f = [\{([MgCl_2]^{\alpha}) /$

$([Mg^{2+}]^{\alpha}_{1/2})\}$ / $\{1+([MgCl_2]^{\alpha})$ / $([Mg^{2+}]^{\alpha}_{1/2})\}]$ where $[Mg^{2+}]_{1/2}$ is the concentration of $MgCl_2$ required for half-maximal folding and α is the Hill coefficient. ΔG values were derived from midpoints of the titration curves using the equation: $\Delta G = -\alpha RTln([Mg^{2+}]_{1/2})$, where α is the Hill coefficient (to account for uptake of Mg^{2+} during folding) and $[Mg^{2+}]_{1/2}$ is the concentration of $MgCl_2$ required for half-maximal folding[18].

Radiolabeled P4–P6 RNA (10–50 nM) was incubated in 1× Tris-borate (TB) buffer (89 mM Tris and 89 mM boric acid, pH 8.5), 5% (v/v) glycerol and 0.1–10 mM $MgCl_2$ for 10 min at 50 °C and 10–20 min at 37 °C then loaded onto 10% polyacrylamide gels. Gels were run 2–3 h at 37 °C in 1× TB and 0.1–10 mM $MgCl_2$.

Nitrocellulose filter binding experiments. RNA–protein binding was assayed as described[22]. A trace quantity (< 5 pM) of 5′ ^{32}P end-labeled RNA was incubated with varying concentrations of *Escherichia coli* Ffh M domain (amino acids 328–432) in a buffer containing 20 mM K-HEPES, pH 7.5, 200 mM KCl, 10 mM $MgCl_2$, 0.5 mM Na-EDTA, 0.01% v/v Igepal C-680 and 0.1 μg ml^{-1} tRNA. Reactions were equilibrated for 1 h prior to applying to filters. Free and bound RNA retained on the filters was quantified by phosphorimaging and analyzed with ImageQuant software (Molecular Dynamics). The data were fit to a Langmuir isotherm (Θ = [protein] / [protein] + K_d) using nonlinear least squares analysis.

Molecular modeling. Mutants of the P4–P6 domain were modeled based on the X-ray crystal structure of the wild type domain using the program MANIP[29]. Models were subsequently refined using the program NUCLIN/NUCLSQ[30]. Buried surface area calculations were performed using the program CNS using a probe radius of 1.4 Å (ref. 31).

Phylogenetic covariation analysis. The 74 aligned sequences of 23S rRNAs provided by the Ribosomal Database Project[32] were analyzed with the program COSEQ (C. Massire and E. Westhof, unpublished results), which enables searching for covariations between a single base and a given base pair. Covariations were analyzed between the residue corresponding to the adenosine and the residues corresponding to the base pair of each Type I and Type II base triple within 23 different Type I/II interactions in *H. marismortui* 23S rRNA. Matrices of residue distributions were generated for each base triple and then combined to generate a matrix of residue distributions for all 23 Type I and Type II base triples. An independent analysis was performed using base pair frequency information provided by the Comparative RNA Web Site (*http://www.rna.icmb.utexas.edu*) using sequences from all three kingdoms. The unavailability of the individual aligned sequences did not allow searches for phylogenetic covariations between the base pair and the adenosine of the base triples. Thus, the data used for this analysis may include sequences in which Type I and Type II interactions do not occur.

Acknowledgments

We thank P. Nissen, J. Ippolito and T. Steitz for helpful discussions. This work was supported by the NIH and the David and Lucile Packard Foundation. E.A.D. was supported in part by NIH training grant. R.T.B was supported by a Jane Coffin Childs postdoctoral fellowship.

Correspondence should be addressed to J.A.D. *email: jennifer.doudna@yale.edu*

Received 23 October, 2000; accepted 1 February, 2001.

1. Leontis, N.B. & Westhof, E. *Q. Rev. Biophys.* **31**, 399–455 (1998).
2. Cate, J.H. *et al. Science* **273**, 1678–1685 (1996).
3. Westhof, E., Dumas, P. & Moras, D. *Acta. Crystallogr. A* **44**, 112–123 (1988).
4. Ferre-D'Amare, A.R., Zhou, K. & Doudna, J.A. *Nature* **395**, 567–574 (1998).
5. Conn, G.L., Draper, D.E., Lattman, E.E. & Gittis, A.G. *Science* **284**, 1171–1174 (1999).
6. Wimberly, B.T., Guymon, R., McCutcheon, J.P., White, S.W. & Ramakrishnan, V. *Cell* **97**, 491–502 (1999).
7. Su, L., Chen, L., Egli, M., Berger, J.M. & Rich, A. *Nature Struct. Biol.* **6**, 285–292 (1999).
8. Mao, H., White, S.A. & Williamson, J.R. *Nature Struct. Biol.* **6**, 1139–1147 (1999).
9. Nix, J., Sussman, D. & Wilson, C. *J. Mol. Biol.* **296**, 1235–1244 (2000).
10. Sussman, D., Nix, J.C. & Wilson, C. *Nature Struct. Biol.* **7**, 53–57 (2000).
11. Ban, N., Nissen, P., Hansen, J., Moore, P.B. & Steitz, T.A. *Science* **289**, 905–920 (2000).
12. Pley, H.W., Flaherty, K.M. & McKay, D.B. *Nature* **372**, 111–113 (1994).
13. Wimberly, B.T. *et al. Nature* **407**, 327–339 (2000).
14. Schluenzen, F. *et al. Cell* **102**, 615–623 (2000).
15. Costa, M. & Michel, F. *EMBO J.* **14**, 1276–1285 (1995).
16. Doherty, E.A., Herschlag, D. & Doudna, J.A. *Biochemistry* **38**, 2982–2990 (1999).
17. Abramovitz, D.L., Friedman, R.A. & Pyle, A.M. *Science* **271**, 1410–1413 (1996).
18. Silverman, S.K. & Cech, T.R. *Biochemistry* **38**, 8691–8702 (1999).
19. Xiong, Y. & Sundaralingam, M. *RNA* **6**, 1316–1324 (2000).
20. Saenger, W. *Principles of nucleic acid structure.* (Springer-Verlag, New York; 1984).
21. Michel, F., Ellington, A.D., Couture, S. & Szostak, J.W. *Nature* **347**, 578–580 (1990).
22. Batey, R.T., Rambo, R.P., Lucast, L., Rha, B. & Doudna, J.A. *Science* **287**, 1232–1239 (2000).
23. Nissen, P., Ippolito, J.A., Ban, M., Moore, P.B. & Steitz, T.A. *Proc. Natl. Acad. Sci. USA* **in the press** (2001).
24. Michel, F. & Westhof, E. *J. Mol. Biol.* **216**, 585–610 (1990).
25. Yoshizawa, S., Fourmy, D. & Puglisi, J.D. *Science* **285**, 1722–1725 (1999).
26. Carter, A.P. *et al. Nature* **407**, 340–348 (2000).
27. Gutell, R.R., Weiser, B., Woese, C.R. & Noller, H.F. *Prog. Nucleic. Acid Res. Mol. Biol.* **32**, 155–216 (1985).
28. Woese, C.R., Winker, S. & Gutell, R.R. *Proc. Natl. Acad. Sci. USA* **87**, 8467–8471 (1990).
29. Massire, C. & Westhof, E. *J. Mol. Graph Model* **16**, 255–257 (1998).
30. Westhof, E., Dumas, P. & Moras, D. *J. Mol. Biol.* **184**, 119–145 (1985).
31. Brunger, A.T. *et al. Acta Crystallogr. D* **54**, 905–921 (1998).
32. Maidak, B.L. *et al. Nucleic Acids Res.* **28**, 173–174 (2000).
33. Kleywegt, G.J. *Acta Crystallogr. D* **52**, 842–857 (1996).
34. Nicholls, A., Sharp, K.A. & Honig, B. *Proteins* **11**, 281–296 (1991).